Constraints on the early and late integrated Sachs-Wolfe effects from the Planck 2015 cosmic microwave background anisotropies in the angular power spectra

Giovanni Cabass, Martina Gerbino, Elena Giusarma, Alessandro Melchiorri, Luca Pagano, and Laura Salvati

Physics Department and INFN, Università di Roma "La Sapienza", Piazzale Aldo Moro 2, 00185, Rome, Italy

(Received 29 July 2015; published 29 September 2015)

The integrated Sachs-Wolfe (ISW) effect predicts additional anisotropies in the cosmic microwave background (CMB) due to time variation of the gravitational potential when the expansion of the Universe is not matter dominated. The ISW effect is therefore expected in the early Universe, due to the presence of relativistic particles at recombination, and in the late Universe, when dark energy starts to dominate the expansion. Deviations from the standard picture can be parametrized by $A_{e\mathrm{ISW}}$ and $A_{l\mathrm{ISW}}$, which rescale the overall amplitude of the early and late ISW effects. Analyzing the most recent CMB temperature spectra from the Planck 2015 release, we detect the presence of the early ISW at high significance with $A_{e\mathrm{ISW}} = 1.06 \pm 0.04$ at 68% C.L. and an upper limit for the late ISW of $A_{l\mathrm{ISW}} < 1.1$ at 95% C.L. The inclusion of the recent polarization data from the Planck experiment results in $A_{e\mathrm{ISW}} = 0.999 \pm 0.028$ at 68% C.L., in better agreement with the value $A_{e\mathrm{ISW}} = 1$ of a standard cosmology. When considering the recent detections of the late ISW coming from correlations between CMB temperature anisotropies and weak lensing, a value of $A_{l\mathrm{ISW}} = 0.85 \pm 0.21$ is predicted at 68% C.L., showing 4σ evidence. We discuss the stability of our result in the case of an extra relativistic energy component parametrized by the effective neutrino number N_{eff} and of a CMB lensing amplitude A_{L}.

DOI: 10.1103/PhysRevD.92.063534 PACS numbers: 98.80.Es, 95.30.Sf, 98.80.Jk

I. INTRODUCTION

Already in 1966, only two years after the discovery of the cosmic microwave background (hereafter, CMB) radiation [1], Sachs and Wolfe [2] presented the first computations of the gravitational redshift of CMB photons by linear matter perturbations. This so-called "Sachs-Wolfe" (SW) effect can be identified in two regimes: the non-integrated SW (NISW) effect and the integrated SW effect (ISW). The NISW is the predominant source of fluctuations in the CMB on scales larger than $\sim 10°$. This effect measured for the first time by the COBE satellite in 1992 [3] occurs at the last scattering surface and provides the first indication for a nearly scale invariant spectrum of primordial fluctuations, as expected in inflationary theory (see e.g. [4,5]).

The ISW, on the contrary, is a "secondary" source of CMB fluctuations, always subdominant with respect to primary sources: it is produced between the last scattering surface and today, and it gives a nonzero contribution only if the expansion of the Universe is not entirely driven by a nonrelativistic matter component. Therefore it will be present after CMB decoupling (produced by the non-negligible relativistic energy component in the total energy density—early ISW), and at recent times when the expansion of the Universe starts to be affected by dark energy (late ISW).

Both *e*ISW and *l*ISW provide an excellent probe for "new physics." A measurement of a late ISW is indeed evidence for a nondark matter dominated expansion of the late Universe, confirming the existence of a "dark energy" component. The *l*ISW combined with other cosmological observables could also be used to constrain dark energy parameters as its equation of state or effective sound speed (see e.g. [6–8]). Moreover, the use of the *l*ISW to constrain the neutrino mass has been proposed by [9].

The *e*ISW, on the contrary, probes the amount of energy stored in relativistic degrees of freedom at recombination. The presence of extra-light particles like sterile neutrinos or thermal axions at such epoch, then, can change its amplitude. The early ISW can also be used to constrain modified gravity models as discussed, for example, in [10].

The *l*ISW has been detected for the first time in [11] by cross-correlating the map of the CMB sky measured by the WMAP satellite with number counts of radio galaxies in the NVSS survey and with the hard x-ray background measured by the HEAO-1 satellite.

This detection has then been confirmed several times in the past years by cross-correlations with different data sets [12–20]. The last analysis obtained by the Planck Collaboration [21] found an $\sim 4\sigma$ indication for *l*ISW, with an amplitude in agreement with a cosmological constant making up the entirety of the dark energy component.

The *e*ISW cannot be probed directly, but it affects the CMB angular spectrum of temperature anisotropies (see e.g. [22] and the discussion in the next section). Constraints on the amplitude of the *e*ISW coming from the WMAP satellite have been presented in [22].

In this paper we present new constraints on the *l*ISW and the *e*ISW effects from the recent measurements of the CMB

temperature and polarization angular power spectrum provided by the Planck satellite, and also discuss degeneracies with other parameters. Most notably, we found a correlation between the amplitude of the *e*ISW and the effective lensing parameter $A_{\rm L}$ in discrepancy with the standard value at ~ 2 standard deviations.

The paper is organized as follows: In the next section we describe the physics of the ISW effect and the parametrization we have used. In Sec. III we present our data analysis method, in Sec. IV we discuss our results and, finally, in Sec. V we derive our conclusions.

II. THE ISW EFFECT

The ISW effect is a contribution to the CMB temperature anisotropy given by the interaction of photons with time-dependent gravitational potentials. At multipole ℓ and linear order in temperature perturbations one has that [23]

$$\Theta_\ell^{\rm ISW}(k) = \int_0^{\eta_0} {\rm d}\eta e^{-\tau(\eta)} \{\dot{\Psi}(k,\eta) - \dot{\Phi}(k,\eta)\} j_\ell(k\Delta\eta), \quad (1)$$

where τ is the optical depth, η_0 is the current conformal time and $\Delta\eta \equiv \eta_0 - \eta$. For times much earlier than recombination ($\eta \ll \eta_{\rm rec}$), CMB photons are tightly coupled to electrons and protons by Compton scattering: this makes $e^{-\tau(\eta)}$ small enough that the ISW effect is negligible.

A. Early ISW: Theory

Equation (1) shows how there is a nonvanishing ISW effect in the presence of time-dependent gravitational potentials Ψ and Φ. For modes that cross the horizon well into matter domination, the gravitational potentials are constant in time. So one expects the ISW to be mainly present at times after recombination (since the energy density of relativistic matter is still considerable at that time). Because of this, one can estimate its contribution to multipole ℓ by evaluating the Bessel function at $\eta \sim \eta_{\rm rec}$: the result is (approximating $\Phi \approx -\Psi$),

$$\Theta_\ell^{e{\rm ISW}}(k) \approx 2 j_\ell(k\Delta\eta_{\rm rec}) \{\Psi(k,\eta_{\rm MD}) - \Psi(k,\eta_{\rm rec})\}, \quad (2)$$

where $\eta_{\rm MD}$ is a time late at matter domination. From Eq. (2) one can see that [24] the early ISW adds in phase with the Sachs-Wolfe primary anisotropy given by

$$\Theta_\ell^{\rm SW}(k) = j_\ell(k\Delta\eta_{\rm rec}) \{\Theta_0(k,\eta_{\rm rec}) + \Psi(k,\eta_{\rm rec})\}. \quad (3)$$

We can see this from the fact that both anisotropies are multiplied by the same Bessel function. This will increase the height of the first acoustic peaks, with the first one being boosted more than the others. The reason is that at times right after recombination, perturbations with $k \ll 1/\eta_{\rm rec}$ do not evolve, while perturbations with $k \gg 1/\eta_{\rm rec}$ are averaged out when integrated along the photon trajectory. This means that the dominant contribution to the early ISW effect is due to perturbations with $k \sim 1/\eta_{\rm rec}$ that approximately corresponds to the first acoustic peak; the effect of $\Theta_\ell^{e{\rm ISW}}(k)$ on the angular anisotropy C_ℓ is suppressed by the factor

$$\frac{\rho_{\rm rad}^2(\eta_{\rm rec})}{\rho_{\rm m}^2(\eta_{\rm rec})} = \left(\frac{1+z_{\rm rec}}{1+z_{\rm eq}}\right)^2. \quad (4)$$

Therefore, even if neutrinos and other relativistic species decoupled from the primordial plasma earlier than the photons, the ISW will still depend on the number of relativistic degrees of freedom at recombination: an increase of the amount of radiation during this epoch (i.e. an effective number of relativistic species $N_{\rm eff} > 3.046$) will delay the advent of matter domination, make $z_{\rm eq}$ smaller, and result in a larger amplitude of the early ISW effect.

This is one of the main reasons why the cosmic microwave background is sensitive to the redshift of matter-radiation equality (and then to the amount of radiation at recombination), thus opening the possibility of constraining the number of extra relativistic species with CMB experiments.

B. Late ISW: Theory

The late ISW effect is active at more recent times, when dark energy starts to play a role and the gravitational potentials are decreasing, and its contribution to the CMB power spectrum is sizable at large scales only [25]. The observable effects of the ISW, in the times dominated by dark energy, are mainly the following [26]:

(i) Focusing on scales corresponding to galaxy clusters, where gravitational perturbations start growing, the CMB photons experience an ISW effect caused by the time dependence of the gravitational potential inside these nonlinear structures. Therefore one expects to find a correlation between $C_\ell^{\rm ISW}$ and the density contrast observed by surveys [27,28]. These correlations can be used to distinguish between the standard ΛCDM universe and models that try to explain the present day acceleration through modifications of gravity [29,30].

(ii) The gravitational potentials that redshift CMB photons (late ISW) are the same that cause the weak lensing distortions: the interplay between these two effects gives rise to a non-Gaussian contribution, which is encoded in the lensing-induced bispectrum between small and large angular scales [31].

The correlation with these large-scale structure (LSS) tracers has been investigated in [21], which studied the cross-correlations of the temperature anisotropies with both lensing potential and galaxy number counts, showing that they yield a 4σ detection of the late ISW. More precisely, temperature-lensing correlations result in $A_{l{\rm ISW}} = 1.04 \pm 0.33$, while including galaxy number counts gives $A_{l{\rm ISW}} = 1.00 \pm 0.25$.

C. Parametrization of early and late ISW effects

In this paper we consider a parametrization of the ISW amplitude in terms of two parameters $A_{e\mathrm{ISW}}$ and $A_{l\mathrm{ISW}}$, which rescale the contribution at early ($A_{e\mathrm{ISW}}$) and late ($A_{l\mathrm{ISW}}$) times in the following way: we introduce in the integrand of Eq. (1) a function $f(\eta)$ given by

$$f(\eta) = \begin{cases} A_{e\mathrm{ISW}} & \text{for } z > 30, \\ A_{l\mathrm{ISW}} & \text{for } z < 30, \end{cases} \tag{5}$$

where the standard scenario is given by $A_{e\mathrm{ISW}} = A_{l\mathrm{ISW}} = 1$. The reason why we have chosen $z = 30$ as a turning point between the early and late contributions is merely a phenomenological one: plotting the integrand of Eq. (1) as a function of redshift with the CAMB code [32], one can see that its minimum lies near $z = 30$.

III. DATA ANALYSIS METHOD

We perform a Markov chain Monte Carlo analysis, making use of the publicly available code COSMOMC [33,34]. Our baseline model is the standard six-parameter ΛCDM model, which includes the baryon density $\Omega_b h^2$, the cold dark matter density $\Omega_c h^2$, the sound horizon angular scale θ, the reionization optical depth τ, the amplitude and spectral index of the primordial power spectrum of scalar perturbations $\ln[10^{10}A_s]$, and n_s. We then include the two amplitudes $A_{e\mathrm{ISW}}$ and $A_{l\mathrm{ISW}}$ of Eq. (5).

We first fix one of the two amplitudes to the standard expected value and let the second one vary freely, but also explore the case of the two amplitudes varying jointly. In addition, we consider other one-parameter extensions to this $\Lambda\mathrm{CDM}+A_{\mathrm{ISW}}$ model, by varying separately the gravitational lensing amplitude A_{L} [35], the primordial helium abundance Y_P (assuming it to be an independent parameter in a nonstandard Big Bang nucleosynthesis (BBN) framework), and T_{CMB} (the blackbody temperature of the CMB at the current epoch). When not varied, these parameters are fixed in agreement with the standard cosmological scenario, namely,

(i) $A_{\mathrm{L}} = 1$,
(ii) $N_{\mathrm{eff}} = 3.046$,
(iii) Y_P as a function of $\Omega_b h^2$ and the effective number of relativistic species N_{eff} equal to 3.046 (as expected from the standard BBN),
(iv) $T_0 = 2.7255$ K [36].

We impose flat priors, but also check the impact of a Gaussian prior $A_{l\mathrm{ISW}} = 1.00 \pm 0.25$ (which will be denoted by the "prior" label in the following plots and tables). This prior is consistent with the 68% C.L. bounds on the same parameter from [21], where the ISW-lensing bispectrum induced on the Gaussian CMB anisotropies by the lensing effect is estimated by cross-correlating the

TABLE I. Constraints at 68% C.L. on the cosmological parameters in the extended ΛCDM model explored here using the *Planck* TT + lowP data set.

Parameter	$\Lambda\mathrm{CDM}+A_{e\mathrm{ISW}}$	$\Lambda\mathrm{CDM}+N_{\mathrm{eff}}+A_{e\mathrm{ISW}}$	$\Lambda\mathrm{CDM}+A_{\mathrm{L}}+A_{e\mathrm{ISW}}$
$\Omega_{\mathrm{b}}h^2$	0.0218 ± 0.0004	0.0218 ± 0.0005	0.0225 ± 0.0005
$\Omega_{\mathrm{c}}h^2$	0.1201 ± 0.0022	0.1204 ± 0.0039	0.1170 ± 0.0027
100θ	1.04072 ± 0.00049	1.04071 ± 0.00056	1.04126 ± 0.00056
τ	0.076 ± 0.019	0.077 ± 0.022	0.059 ± 0.020
n_{s}	0.9724 ± 0.0080	0.974 ± 0.016	0.9750 ± 0.0081
$\ln[10^{10}A_{\mathrm{s}}]$	3.080 ± 0.037	3.083 ± 0.048	3.045 ± 0.041
N_{eff}	$\equiv 1$	$3.08^{+0.29}_{-0.34}$	$\equiv 3.046$
A_{L}	$\equiv 1$	$\equiv 1$	1.216 ± 0.11
$A_{e\mathrm{ISW}}$	$1.064^{+0.042}_{-0.043}$	1.065 ± 0.043	1.018 ± 0.046

TABLE II. Constraints at 68% C.L. on extensions of the ΛCDM model for the *Planck* TT, TE, EE + lowP data set.

Parameter	$\Lambda\mathrm{CDM}+A_{e\mathrm{ISW}}$	$\Lambda\mathrm{CDM}+N_{\mathrm{eff}}+A_{e\mathrm{ISW}}$	$\Lambda\mathrm{CDM}+A_{\mathrm{L}}+A_{e\mathrm{ISW}}$
$\Omega_{\mathrm{b}}h^2$	0.0222 ± 0.0002	0.0222 ± 0.0003	0.0225 ± 0.0002
$\Omega_{\mathrm{c}}h^2$	0.1199 ± 0.0015	0.1189 ± 0.0031	$0.1183^{+0.0016}_{-0.0015}$
100θ	1.04072 ± 0.00031	1.04087 ± 0.00045	1.04095 ± 0.00032
τ	0.081 ± 0.017	0.080 ± 0.018	$0.056^{+0.021}_{-0.020}$
n_{s}	0.9638 ± 0.0058	0.961 ± 0.010	0.967 ± 0.0055
$\ln[10^{10}A_{\mathrm{s}}]$	3.098 ± 0.033	3.091 ± 0.038	$3.042^{+0.043}_{-0.040}$
N_{eff}	$\equiv 1$	$2.99^{+0.20}_{-0.21}$	$\equiv 3.046$
A_{L}	$\equiv 1$	$\equiv 1$	$1.182^{+0.076}_{-0.086}$
$A_{e\mathrm{ISW}}$	0.999 ± 0.028	1.002 ± 0.028	0.988 ± 0.027

Planck CMB maps with the Planck map of the lensing potential [21].

We test the following data sets: the high-ℓ Planck temperature and polarization power spectra in the range $30 \leq \ell < 2500$ (hereafter *Planck* TT and *Planck* TT, TE, EE) combined with the low-ℓ Planck temperature and polarization power spectra in the range $2 \leq \ell < 29$ (denoted as lowP) [37]. Regarding polarization spectra at high ℓ, we also test the WMAP power spectra in temperature and polarization [38] up to $\ell = 1200$. When T_0 is varied, we also add information from baryon acoustic oscillation (BAO) as reported in [39], in order to break degeneracies among cosmological parameters.

IV. RESULTS

A. Early ISW: Results

We start from considering the case in which only the early ISW effect is left free to vary. The results of our analysis are shown in Tables I and II in which we report the 68% C.L. around the mean value of the posterior.

By comparing the results given in the first column of Table I with those shown by the Planck Collaboration in [39] for a ΛCDM model, it can be noticed that the most interesting effects which arise from the inclusion of $A_{e\mathrm{ISW}}$ as a free parameter are on the parameters $\Omega_\mathrm{b}h^2$ and n_s: a lower $\Omega_\mathrm{b}h^2$ and a higher n_s than the standard ΛCDM case are favored.

This can be understood looking at Fig. 1, which shows the correlation between $A_{e\mathrm{ISW}}$ with $\Omega_\mathrm{b}h^2$ and n_s. A larger $A_{e\mathrm{ISW}}$ or a larger $\Omega_\mathrm{b}h^2$ act in (almost) the same way on the CMB spectrum, increasing the height of the peaks at $\ell \sim 100$. This is reflected in the strong degeneracy between $A_{e\mathrm{ISW}}$ and $\Omega_\mathrm{b}h^2$ (left panel of Fig. 1); in fact a higher value of $A_{e\mathrm{ISW}}$ can be compensated by a decrease of $\Omega_\mathrm{b}h^2$ to keep fixed the height of the acoustic

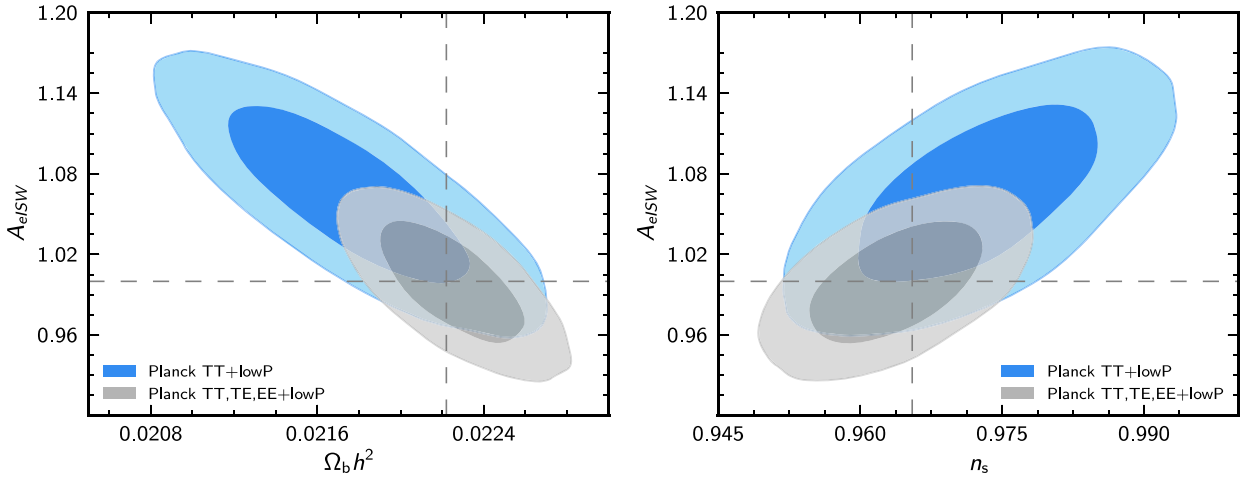

FIG. 1 (color online). Two-dimensional posterior probability in the $(\Omega_\mathrm{b}h^2, A_{e\mathrm{ISW}})$ and $(n_\mathrm{s}, A_{e\mathrm{ISW}})$ planes for the *Planck* TT + lowP data set and the *Planck* TT, TE, EE + lowP data sets.

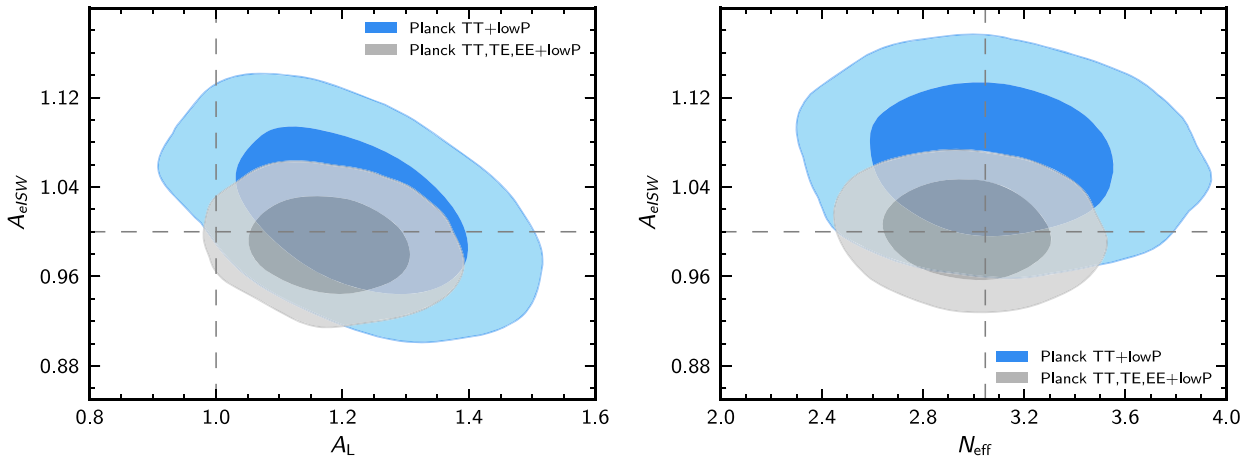

FIG. 2 (color online). The left panel depicts the 68% and 95% C.L. allowed regions in the $(A_\mathrm{L}, A_{e\mathrm{ISW}})$ plane for the *Planck* TT + lowP and the *Planck* TT, TE, EE + lowP data sets. The right panel shows the 68% and 95% C.L. regions in the $(N_\mathrm{eff}, A_{e\mathrm{ISW}})$ plane.

TABLE III. Constraints at 68% C.L. on the amplitude of the early-time ISW effect, $A_{e\mathrm{ISW}}$, for the different combinations of data sets and models.

Extended model ΛCDM+	$A_{e\mathrm{ISW}}$
$A_{e\mathrm{ISW}}$	
WMAP	$1.007^{+0.056}_{-0.058}$
Planck TT + lowP	$1.064^{+0.042}_{-0.043}$
Planck TT, TE, EE + lowP	0.999 ± 0.028
$A_{e\mathrm{ISW}} + A_{\mathrm{L}}$	
Planck TT + lowP	1.018 ± 0.046
Planck TT, TE, EE + lowP	0.988 ± 0.027
$A_{e\mathrm{ISW}} + N_{\mathrm{eff}}$	
Planck TT + lowP	1.065 ± 0.043
Planck TT, TE, EE + lowP	1.002 ± 0.028
$A_{e\mathrm{ISW}} + n_{\mathrm{run}}$	
Planck TT + lowP	$1.066^{+0.041}_{-0.042}$
Planck TT, TE, EE + lowP	$1.004^{+0.027}_{-0.031}$
$A_{e\mathrm{ISW}} + Y_P$	
Planck TT + lowP	1.066 ± 0.042
Planck TT, TE, EE + lowP	1.000 ± 0.028
$A_{e\mathrm{ISW}} + T_{\mathrm{CMB}}$	
Planck TT + lowP + BAO	1.063 ± 0.046
Planck TT, TE, EE + lowP + BAO	1.001 ± 0.028

peaks of the CMB. The right panel of Fig. 1 shows the 68% C.L. and 95% C.L. allowed regions in the $(n_{\mathrm{s}}, A_{e\mathrm{ISW}})$ plane: as the value of n_{s} increases, a larger $A_{e\mathrm{ISW}}$ is also allowed.

When we consider the *Planck* TT, TE, EE + lowP data sets (first column of Table II) the bounds on the optical depth τ and the amplitude of the primordial spectrum $\ln[10^{10}A_s]$ are displaced to higher values and the errors on the cosmological parameters are reduced.

Instead, as shown in Tables I and II, the inclusion of gravitational lensing A_{L} and of the effective number of relativistic species N_{eff} does not change significantly the constraints on the parameters with respect to those obtained by the Planck Collaboration [39]. Figure 2, left panel, depicts the 68% and 95% C.L. allowed regions in the $(A_{\mathrm{L}}, A_{e\mathrm{ISW}})$ plane. Even if the early ISW and weak lensing operate at very different scales, the latter is also sensitive to the matter density $\Omega_{\mathrm{m}}h^2$ [40]: this explains the mild correlation between these two parameters shown in the left panel. The right panel of Fig. 2 illustrates the 68% and 95% C.L. contours in the $(N_{\mathrm{eff}}, A_{e\mathrm{ISW}})$ plane resulting from the analysis of CMB data. Notice that, in contrast to what was said in Sec. II A, these parameters appear uncorrelated. Actually, instead, this agrees with the conclusions of [41], in which the authors explain how a Y_P "fixed" by BBN consistency would not degrade the constraint on N_{eff}, even if $A_{e\mathrm{ISW}}$ is left free to vary.

Table III depicts the 68% C.L. constraints on $A_{e\mathrm{ISW}}$ for the different cosmological models explored in this study using different cosmological data. First, notice that the *Planck* TT + lowP data alone already provide tighter constraints than WMAP on $A_{e\mathrm{ISW}}$. Using only the *Planck* TT + lowP data, we can see that the inclusion of the lensing amplitude A_{L} as a free parameter (in addition to the standard ΛCDM picture) tends to diminish the 1σ indication for an $A_{e\mathrm{ISW}} \neq 1$. We also note that this preference persists when we vary other parameters like the effective number of relativistic species N_{eff}, the running of the scalar tilt n_{run}, and the helium mass fraction Y_P. On the other hand, it vanishes when we consider the *Planck* TT, TE, EE + lowP data for all different cosmological models. These results are also summarized by the plots of

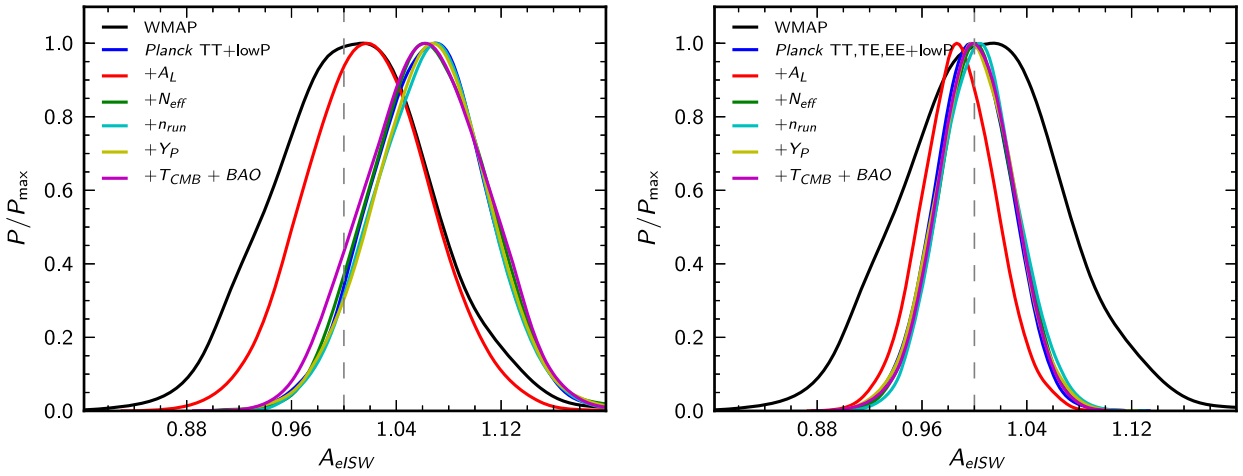

FIG. 3 (color online). One-dimensional posterior probability for the amplitude of the early-time ISW effect for the indicated data sets and models. The black and blue curves correspond to a ΛCDM + $A_{e\mathrm{ISW}}$ model. The additional curves come from the indicated one-parameter extension to this baseline model, for the *Planck* TT + lowP data set (left) and *Planck* TT, TE, EE + lowP data set (right). When T_{CMB} is varied, BAO data sets [42–46] are included in the analysis, in order to break degeneracies between cosmological parameters.

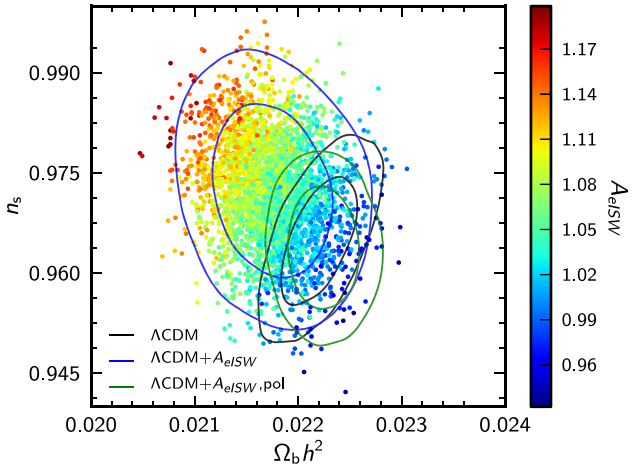

FIG. 4 (color online). Two-dimensional contours in the $\Omega_b h^2 - n_S$ plane, colored by the value of the parameter A_{eISW}, for the *Planck* TT + lowP and *Planck* TT, TE, EE + lowP data sets. The black and blue contours show the two-dimensional posterior probability in the $\Omega_b h^2 - n_S$ plane for the same data set and the indicated models. The green contours include the addition of high-ℓ polarization.

Fig. 3 showing the one-dimensional posteriors for A_{eISW} in the various extensions of the ΛCDM we discussed.

Figure 4 shows the 2D marginalized posterior distribution for $\Omega_b h^2$ and n_s using the *Planck* TT + lowP and *Planck* TT, TE,EE+lowP data sets. We consider two different cosmological models: ΛCDM vs ΛCDM $+A_{eISW}$. Notice that the correlation between $\Omega_b h^2$ and n_s turns from positive (ΛCDM) to negative (ΛCDM + A_{eISW}). This is due to the strong degeneracy between $\Omega_b h^2$ and A_{eISW} (already shown in Fig. 1) that reduces the degeneracies between the other parameters of the ΛCDM model. Moreover, if also the information from the Planck high-ℓ polarization data is included, the values of these three parameters tend to come in accord with their standard ΛCDM value (see Table III), even if the direction of the degeneracy between $\Omega_b h^2$ and n_s remains positive.

TABLE IV. Constraints at 68% C.L. (unless otherwise stated) on the amplitude of the late-time ISW effect, A_{lISW}, for the different combinations of data sets and models considered in the text.

Extended model ΛCDM+	A_{lISW}
A_{lISW}	
WMAP	$0.958^{+0.391}_{-0.317}$
Planck TT + lowP	< 1.14 (95% C.L.)
Planck TT, TE, EE + lowP	< 1.11 (95% C.L.)
A_{lISW}, prior	
WMAP	$0.958^{+0.220}_{-0.192}$
Planck TT + lowP	0.853 ± 0.211
Planck TT, TE, EE + lowP	$0.847^{+0.217}_{-0.203}$
$A_{lISW} + N_{eff}$	
Planck TT + lowP	< 1.14 (95% C.L.)
Planck TT, TE, EE + lowP	< 1.11 (95% C.L.)
$A_{lISW} + A_L$	
Planck TT + lowP	< 1.25 (95% C.L.)
Planck TT, TE, EE + lowP	< 1.12 (95% C.L.)

B. Late ISW: Results

In this section we present the results obtained considering only the late ISW effect. Table IV presents the constraints on A_{lISW} for the different cosmological data combinations considered here. Figure 5 contains

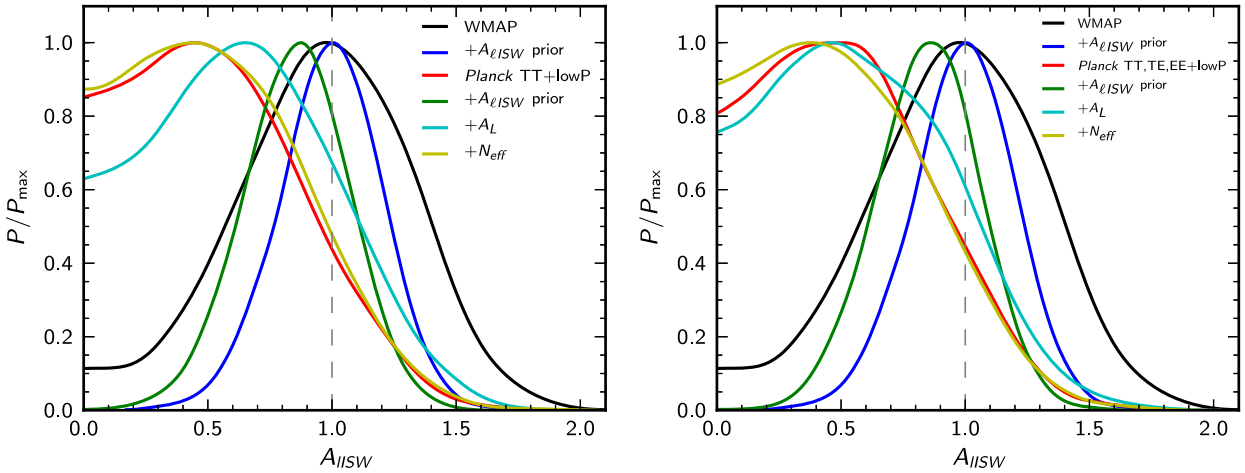

FIG. 5 (color online). One-dimensional posterior probability for the amplitude of the late-time ISW effect for the data sets and models discussed in the text. The black curves refer to a ΛCDM + A_{lISW}, with the WMAP data set for the high-ℓ polarization. The remaining curves include the *Planck* TT + lowP data (left panel), and the *Planck* TT, TE, EE + lowP data (right panel). The "A_{lISW} prior" label indicates the inclusion of the Gaussian prior on A_{lISW} coming from the cross-correlated analysis of the CMB bispectrum and galaxy clusters.

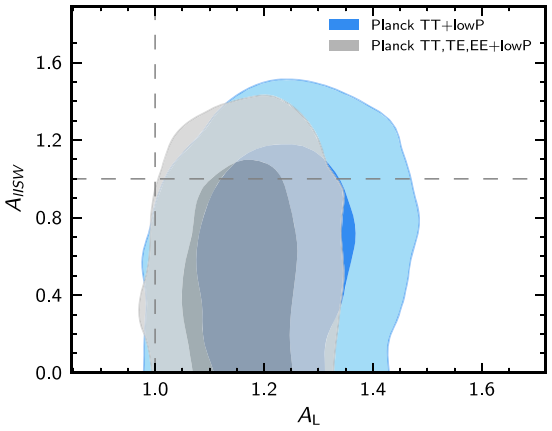

FIG. 6 (color online). Two-dimensional posterior probability in the $A_{\mathrm{L}} - A_{l\mathrm{ISW}}$ plane for the *Planck* TT + lowP and *Planck* TT, TE, EE + lowP data sets. This posterior shows that, while the amplitude of the late ISW effect and the lensing parameter A_{L} are not correlated, the inclusion of high-ℓ polarization data from Planck brings the contours back in accord with $A_{\mathrm{L}} = 1$ and $A_{l\mathrm{ISW}} = 1$.

the one-dimensional posteriors for the amplitude of the late-time ISW effect in the various extensions of ΛCDM model. Notice that when we consider the case with a flat prior on $A_{l\mathrm{ISW}}$, there is consistency with $A_{l\mathrm{ISW}} = 1$ for the WMAP data set. The *Planck* TT + lowP and the *Planck* TT, TE, EE + lowP measurements set the 95% C.L. upper limit of $A_{l\mathrm{ISW}} \lesssim 1.14$ and $A_{l\mathrm{ISW}} \lesssim 1.11$ respectively. We note that Planck alone does not improve significantly the constraint on $A_{l\mathrm{ISW}}$ with respect to WMAP measurements. This occurs because the late-time ISW affects a region of CMB power spectrum multipoles that is dominated by cosmic variance, rather than by instrumental precision. Moreover the bounds on $A_{l\mathrm{ISW}}$ are not affected if the effective number of relativistic species (N_{eff}) is included.

We also consider a Gaussian prior of $A_{l\mathrm{ISW}} = 1.00 \pm 0.25$ from the bispectrum-LSS cross-correlation analysis, which allows us to take into account the constraints on the late ISW coming from LSS measurements. The inclusion of the prior results in a tighter constraint from WMAP, while the posterior on $A_{l\mathrm{ISW}}$ when Planck data set is considered is shifted towards $A_{l\mathrm{ISW}} = 1$.

Figure 6 shows the 68% and 95% C.L. allowed regions in the $(A_{\mathrm{L}}, A_{l\mathrm{ISW}})$ plane for the *Planck* TT + lowP and *Planck* TT, TE, EE + lowP data sets. Notice that there is no correlation between $A_{\mathrm{L}} - A_{l\mathrm{ISW}}$. This was expected since the late ISW is active at low ℓ, while weak lensing operates at high ℓ. Moreover there is a mild preference for a nonstandard value of both parameters. Marginalizing over A_{L} we obtain an upper limit of $A_{l\mathrm{ISW}} < 1.25$ at 95% C.L. using the *Planck* TT + lowP data set, while the inclusion of high-ℓ polarization measurements tightens the constraint at $A_{l\mathrm{ISW}} < 1.12$ at 95% C.L.

C. Early + late ISW

We conclude by considering the case of both $A_{e\mathrm{ISW}}$ and $A_{l\mathrm{ISW}}$ varying jointly. Constraints on these two parameters are reported in Table V. The one-dimensional and two-dimensional posterior probabilities for a selected subset of data sets and models are shown in Fig. 7 and Fig. 8, respectively. As mentioned in Secs. IV A and IV B, when compared with the results from WMAP, the Planck data provide much tighter constraints on $A_{e\mathrm{ISW}}$ even when considering temperature only, while the constraining power on $A_{l\mathrm{ISW}}$ is comparable.

The upper bounds on $A_{l\mathrm{ISW}}$ are well compatible with the standard case for all data sets used, while there is a 1σ preference of $A_{e\mathrm{ISW}} \neq 1$ when using the *Planck* TT + lowP data set. We note, though, that such a preference for $A_{e\mathrm{ISW}} \neq 1$ disappears when we let A_{L} free to vary, as a result of the mild degeneracy between the two parameters discussed in Sec. IV A. Allowing the number of relativistic species to vary does not alter the constraints with respect to the minimal extension to ΛCDM.

The inclusion of small-scale polarization data significantly tightens the constraints on $A_{e\mathrm{ISW}}$, almost halving the posterior width. On the other hand, as already expected, it does not provide further information on $A_{l\mathrm{ISW}}$, as highlighted by the superposition of both the green curves with the solid red one in the top right panel of Fig. 7.

TABLE V. Constraints at 68% C.L. (unless otherwise stated) on the amplitude of the late-time ISW effect $A_{l\mathrm{ISW}}$ and of the early-time ISW effect $A_{e\mathrm{ISW}}$ for the indicated data sets and models.

Data set, model	$A_{l\mathrm{ISW}}$	$A_{e\mathrm{ISW}}$
WMAP, ΛCDM + $A_{l\mathrm{ISW}}$ + $A_{e\mathrm{ISW}}$	$1.011^{+0.434}_{-0.374}$	$1.019^{+0.061}_{-0.066}$
Planck *Planck* TT + lowP, ΛCDM + $A_{l\mathrm{ISW}}$ + $A_{e\mathrm{ISW}}$	< 1.34 (95% C.L.)	1.055 ± 0.044
Planck *Planck* TT + lowP, ΛCDM + $A_{l\mathrm{ISW}}$ + $A_{e\mathrm{ISW}}$ + A_{L}	< 1.32 (95% C.L.)	$1.009^{+0.047}_{-0.048}$
Planck *Planck* TT + lowP, ΛCDM + $A_{l\mathrm{ISW}}$ + $A_{e\mathrm{ISW}}$ + N_{eff}	< 1.35 (95% C.L.)	$1.057^{+0.043}_{-0.044}$
Planck *Planck* TT, TE, EE + lowP, ΛCDM + $A_{l\mathrm{ISW}}$ + $A_{e\mathrm{ISW}}$	< 1.11 (95% C.L.)	$0.994^{+0.027}_{-0.028}$
Planck *Planck* TT, TE, EE + lowP, ΛCDM + $A_{l\mathrm{ISW}}$ + $A_{e\mathrm{ISW}}$ + A_{L}	< 1.12 (95% C.L.)	0.985 ± 0.028
Planck *Planck* TT, TE, EE + lowP, ΛCDM + $A_{l\mathrm{ISW}}$ + $A_{e\mathrm{ISW}}$ + N_{eff}	< 1.10 (95% C.L.)	$0.996^{+0.028}_{-0.030}$

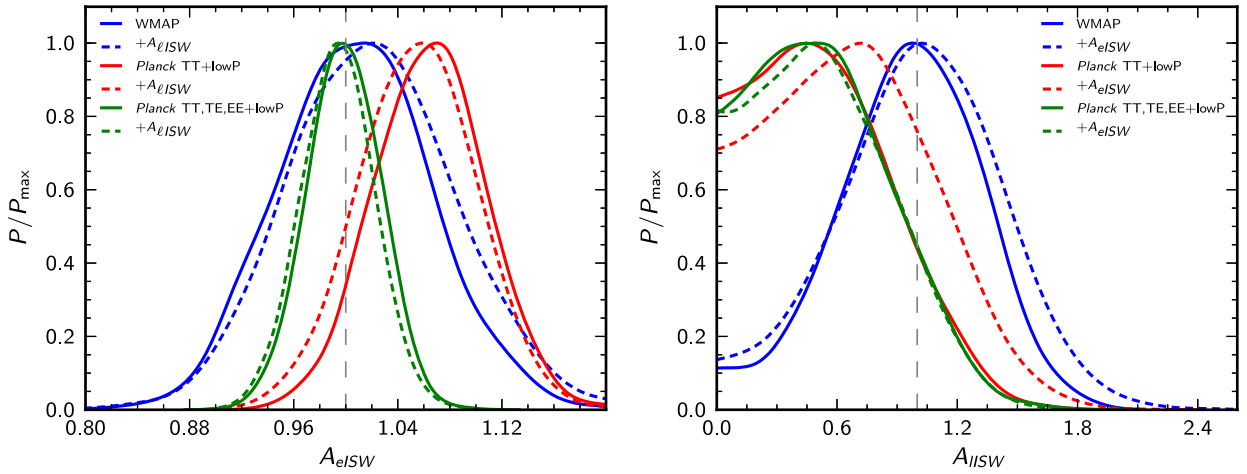

FIG. 7 (color online). One-dimensional posterior probability for the amplitude of the early-time ISW effect (left) and late-time ISW effect (right) for the indicated data sets and models. For each plot, the solid curves have been obtained for the corresponding one-parameter extension to the base ΛCDM model. The dashed curves correspond to the joint variation of $A_{e\mathrm{ISW}}$ and $A_{l\mathrm{ISW}}$.

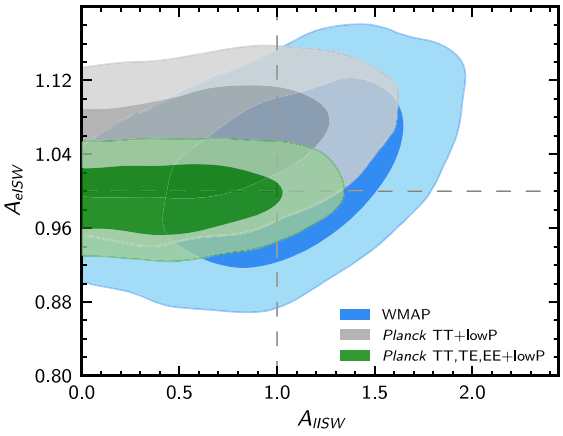

FIG. 8 (color online). Two-dimensional posterior probability in the $A_{l\mathrm{ISW}} - A_{e\mathrm{ISW}}$ plane for the *Planck* TT + lowP and *Planck* TT, TE, EE + lowP data sets.

V. CONCLUSIONS

In this paper we study the constraints on the amplitude of the integrated Sachs-Wolfe effect, both its early- and late-time contributions.

We find that the *Planck* TT + lowP data are consistent with a nonzero early ISW, with an amplitude $A_{e\mathrm{ISW}}$ in agreement with $A_{e\mathrm{ISW}} = 1$ as predicted by theory, with a 1σ preference of $A_{e\mathrm{ISW}} \neq 1$ when considering extensions to the ΛCDM model discussed in this work. We also confirm the strong degeneracy between the amplitude of the early ISW and parameters like $\Omega_b h^2$ and n_S. Our analysis also hints for a correlation between $A_{e\mathrm{ISW}}$ and the lensing parameter A_L.

Regarding the late ISW, Planck data alone place a constraint $A_{l\mathrm{ISW}} \lesssim 1.1$ at 95% C.L. When supplemented with a prior on $A_{l\mathrm{ISW}}$ coming from CMB temperature anisotropy-weak lensing correlations, however, we find an $\sim 4\sigma$ detection $A_{l\mathrm{ISW}} = 0.85 \pm 0.21$.

When we consider also the recent polarization data at high ℓ from the Planck Collaboration, we find that the evidence for a nonstandard value of $A_{e\mathrm{ISW}}$ disappears. The reason is that the addition of TE and EE spectra leads to a better agreement of data with the standard ΛCDM model. More precisely, $A_{e\mathrm{ISW}}$ gets dragged towards 1 through its degeneracy with $\Omega_b h^2$ and n_s, which return in agreement with the ΛCDM best fit when polarization is included.

On the other hand, using the small-scale polarization spectra does not change the results obtained for $A_{l\mathrm{ISW}}$. Their effect is to slightly tighten the upper bounds obtained when considering only the temperature spectra.

When the two parameters are allowed to vary jointly, the same pattern described above is reproduced.

ACKNOWLEDGMENTS

We would like to thank Antony Lewis for the use of the numerical codes COSMOMC and CAMB. We acknowledge support by Theoretical Astroparticle Physics research Grant No. 2012CPPYP7 under the program PRIN 2012 funded by MIUR and by TASP, iniziativa specifica INFN.

[1] A. A. Penzias and R. W. Wilson, Astrophys. J. **142**, 419 (1965).
[2] R. K. Sachs and A. M. Wolfe, Astrophys. J. **147**, 73 (1967) Gen. Relativ. Gravit. **39**, 1929 (2007).
[3] G. F. Smoot, C. L. Bennett, A. Kogut, E. L. Wright, J. Aymon, N. W. Boggess, E. S. Cheng, G. De Amici *et al.*, Astrophys. J. **396**, L1 (1992).
[4] A. R. Liddle and D. H. Lyth, Phys. Rep. **231**, 1 (1993).
[5] J. E. Lidsey, A. R. Liddle, E. W. Kolb, E. J. Copeland, T. Barreiro, and M. Abney, Rev. Mod. Phys. **69**, 373 (1997).
[6] P. S. Corasaniti, T. Giannantonio, and A. Melchiorri, Phys. Rev. D **71**, 123521 (2005).
[7] P. Vielva, E. Martinez-Gonzalez, and M. Tucci, Mon. Not. R. Astron. Soc. **365**, 891 (2006).
[8] J. D. McEwen, P. Vielva, M. P. Hobson, E. Martinez-Gonzalez, and A. N. Lasenby, Mon. Not. R. Astron. Soc. **376**, 1211 (2007).
[9] J. Lesgourgues, W. Valkenburg, and E. Gaztanaga, Phys. Rev. D **77**, 063505 (2008).
[10] P. Zhang, Phys. Rev. D **73**, 123504 (2006).
[11] S. Boughn and R. Crittenden, Nature (London) **427**, 45 (2004).
[12] R. Scranton *et al.* (SDSS Collaboration), arXiv:astro-ph/0307335.
[13] P. Fosalba, E. Gaztanaga, and F. Castander, Astrophys. J. **597**, L89 (2003).
[14] M. R. Nolta *et al.* (WMAP Collaboration), Astrophys. J. **608**, 10 (2004).
[15] N. Afshordi, Y. S. Loh, and M. A. Strauss, Phys. Rev. D **69**, 083524 (2004).
[16] T. Giannantonio, R. G. Crittenden, R. C. Nichol, R. Scranton, G. T. Richards, A. D. Myers, R. J. Brunner, A. G. Gray *et al.*, Phys. Rev. D **74**, 063520 (2006).
[17] A. Rassat, K. Land, O. Lahav, and F. B. Abdalla, Mon. Not. R. Astron. Soc. **377**, 1085 (2007).
[18] S. Ho, C. Hirata, N. Padmanabhan, U. Seljak, and N. Bahcall, Phys. Rev. D **78**, 043519 (2008).
[19] T. Giannantonio, R. Scranton, R. G. Crittenden, R. C. Nichol, S. P. Boughn, A. D. Myers, and G. T. Richards, Phys. Rev. D **77**, 123520 (2008).
[20] P. A. R. Ade *et al.* (Planck Collaboration), Astron. Astrophys. **571**, A19 (2014).
[21] P. A. R. Ade *et al.* (Planck Collaboration), arXiv:1502.01595.
[22] Z. Hou, R. Keisler, L. Knox, M. Millea, and C. Reichardt, Phys. Rev. D **87**, 083008 (2013).
[23] We use the Newtonian gauge convention $g_{00} = -1 - 2\Psi$ and $g_{ij} = a^2\delta_{ij}(1 + 2\Phi)$.
[24] R. Bowen, S. H. Hansen, A. Melchiorri, J. Silk, and R. Trotta, Mon. Not. R. Astron. Soc. **334**, 760 (2002).
[25] At the present time the relevant length of photon trajectories is comparable to the horizon size, so that the main contribution to Eq. (1) comes from perturbations with $\lambda \sim \eta_0$ (the contributions of shorter wavelengths again average away). Therefore the late ISW effect influences only multipoles corresponding to $k \sim 1/\eta_0$, that is $\ell \sim 1$.
[26] A. Manzotti and S. Dodelson, Phys. Rev. D **90**, 123009 (2014).
[27] P. S. Corasaniti, T. Giannantonio, and A. Melchiorri, Phys. Rev. D **71**, 123521 (2005).
[28] A. Cabre, E. Gaztanaga, M. Manera, P. Fosalba, and F. Castander, Mon. Not. R. Astron. Soc. **372**, L23 (2006).
[29] A. Lue, R. Scoccimarro, and G. Starkman, Phys. Rev. D **69**, 044005 (2004).
[30] E. Di Valentino, A. Melchiorri, V. Salvatelli, and A. Silvestri, Phys. Rev. D **86**, 063517 (2012).
[31] W. Hu and T. Okamoto, Astrophys. J. **574**, 566 (2002).
[32] http://camb.info.
[33] A. Lewis, Phys. Rev. D **87**, 103529 (2013).
[34] A. Lewis and S. Bridle, Phys. Rev. D **66**, 103511 (2002).
[35] E. Calabrese, A. Slosar, A. Melchiorri, G. F. Smoot, and O. Zahn, Phys. Rev. D **77**, 123531 (2008).
[36] D. J. Fixsen, Astrophys. J. **707**, 916 (2009).
[37] N. Aghanim *et al.* (Planck Collaboration), arXiv:1507.02704.
[38] C. L. Bennett *et al.*, Astrophys. J. Suppl. Ser. **208**, 20B (2013).
[39] P. A. R. Ade *et al.* (Planck Collaboration).
[40] P. A. R. Ade *et al.* (Planck Collaboration).
[41] Z. Hou, R. Keisler, L. Knox, M. Millea, and C. Reichardt, Phys. Rev. D **87**, 083008 (2013).
[42] W. J. Percival *et al.* (SDSS Collaboration), Mon. Not. R. Astron. Soc. **401**, 2148 (2010).
[43] F. Beutler, C. Blake, M. Colless, D. H. Jones, L. Staveley-Smith, L. Campbell, Q. Parker, W. Saunders, and F. Watson, Mon. Not. R. Astron. Soc. **416**, 3017 (2011).
[44] C. Blake, E. Kazin, F. Beutler, T. Davis, D. Parkinson, S. Brough, M. Colless, C. Contreras *et al.*, Mon. Not. R. Astron. Soc. **418**, 1707 (2011).
[45] N. Padmanabhan, X. Xu, D. J. Eisenstein, R. Scalzo, A. J. Cuesta, K. T. Mehta, and E. Kazin, Mon. Not. R. Astron. Soc. **427**, 2132 (2012).
[46] L. Anderson, E. Aubourg, S. Bailey, D. Bizyaev, M. Blanton, A. S. Bolton, J. Brinkmann, J. R. Brownstein *et al.*, Mon. Not. R. Astron. Soc. **427**, 3435 (2012).